Article

Discovery Medicine 2026; 38(205): 491–504
https://doi.org/10.24976/Discov.Med.202638205.41

Function and Mechanism of SLC38A5 in Retinoblastoma Development

Chao Wu[1], Yan Deng[1], Xiaoyan Xiong[1], Ying Lu[1], Xiaolong Yin[1,*]

[1]Department of Ophthalmology, The Second Affiliated Hospital, Jiangxi Medical College, Nanchang University, 330006 Nanchang, Jiangxi, China
*Correspondence: yinxiaolong22216@163.com (Xiaolong Yin)
Submitted: 29 September 2025 Revised: 14 January 2026 Accepted: 20 January 2026 Published: 20 February 2026

Background: Retinoblastoma (RB) is a highly aggressive pediatric ocular malignancy whose molecular mechanisms remain unclear. Although implicated in various cancers, the amino acid transporter Solute Carrier Family 38 Member 5 (SLC38A5) remains uncharacterized in RB. Herein, we aimed to investigate the expression pattern, biological functions, and underlying mechanisms of SLC38A5 in RB.

Methods: SLC38A5 expression was analyzed in human RB cell lines using Western blotting and quantitative real-time polymerase chain reaction (qRT-PCR). Functional characterization was performed through genetic manipulation (knockdown/overexpression) followed by comprehensive phenotypic assessment. *In vivo* xenograft models were used to evaluate tumor growth.

Results: SLC38A5 was significantly overexpressed in RB cell lines, particularly in Y79 and WERI-Rb1 ($p < 0.001$). SLC38A5 knockdown suppressed cell proliferation, migration, and invasion, and induced apoptosis ($p < 0.05$). Conversely, SLC38A5 overexpression enhanced these malignant phenotypes ($p < 0.05$). Additionally, SLC38A5 modulated mitochondrial function via the mTOR signaling pathway ($p < 0.05$). *In vivo*, SLC38A5 overexpression promoted tumor growth, whereas knockdown inhibited tumor progression ($p < 0.05$).

Conclusion: SLC38A5 acts as a key regulator of RB progression by modulating core biological processes, including proliferation, migration, invasion, and mitochondrial function. Targeting SLC38A5 may represent a potential therapeutic strategy for RB.

Keywords: SLC38A5; retinoblastoma; mTOR signaling; mitochondrial function; apoptosis

Introduction

Retinoblastoma (RB) is a malignant tumor originating from retinal neuroepithelium cells [1]. It represents the most prevalent ocular tumor in children, posing a serious threat to the life and vision of affected patients. RB affects approximately one in 15,000 to 20,000 newborns worldwide, with about 95.0% of cases occurring before the age of five [2–4]. China, the most populous country in the world, reports about 1000 new RB cases annually, accounting for one-eighth of all global cases [5]. RB pathogenesis is primarily driven by bi-allelic inactivation of the RB1 tumor suppressor gene, with a few cases caused by *MYCN* gene overexpression [6–8]. Although current treatment methods such as chemotherapy, radiotherapy, and surgery have made significant progress in improving patient survival rates, tumor recurrence and metastasis remain major clinical challenges [9]. Therefore, a deeper investigation into the molecular mechanisms of RB and the identification of new therapeutic targets have become urgent scientific problems.

Amino acid transporters play a crucial role in cellular metabolism and energy balance. Solute Carrier Family 38 Member 5 (SLC38A5) is a key amino acid transporter in the SLC38 family, responsible for the selective transmembrane transport of amino acids [10]. SLC38A5 has been implicated in amino acid uptake, energy metabolism, and the regulation of critical biological functions in tumor cells [11,12]. The role of SLC38A5 in malignant tumors has garnered increasing attention in recent years. In the tumor microenvironment, SLC38A5 supports tumor cell growth, metabolic adaptation, and drug resistance by enhancing glutamine metabolism and regulating related signaling pathways [13]. A study demonstrates that SLC38A5 suppresses ferroptosis and attenuates lipid peroxidation, thereby conferring gemcitabine resistance to pancreatic cancer cells and contributing to poor patient prognosis [14]. Niclosamide, a potent SLC38A5 inhibitor, effectively suppresses mTOR pathway activation by targeting SLC38A5 in Triple-Negative Breast Cancer (TNBC) cells, thereby exerting its anti-tumor effects [15]. However, the expression pattern, function, and underlying mechanisms of SLC38A5 in RB remain largely unknown, particularly its role in cellular processes and potential impact on metabolic reprogramming or signaling pathways.

Herein, we investigate the biological functions and underlying mechanisms of SLC38A5 in RB. These findings

provide mechanistic insights into RB progression and lay the groundwork for future exploration of SLC38A5 as a therapeutic target.

Materials and Methods

Cell Treatment and Transfection

Human retinal cell lines, including WERI-Rb1 (BFB, BFN6021607, Shanghai, China), Y79 (BFB, BFN60700369), SO-Rb50 (BFB, BFN6021608), and normal retinal epithelial cell line ARPE-19 (BFB, BFN60807591), were purchased from the Shanghai Cell Bank. The cells were cultured in DMEM (BFB, BFNP2001A) with 10% FBS (Sangon, E600001, Shanghai, China) and 1% penicillin-streptomycin (Sangon, E607011-0500) at 37 °C in a 5% CO_2 incubator (Thermo Scientific, 311, Waltham, MA, USA). All cell lines were confirmed to be of human origin by STR profiling, with no cross-contamination, and tested negative for mycoplasma.

To investigate the effect of SLC38A5 expression on cell behavior, the target cells were seeded in 24 well plates at a density of 2×10^5 cells per well, and transduced with lentiviral particles when the confluence reached approximately 70%. Cells were transfected with SLC38A5 overexpression (SLC38A5-OE) and SLC38A5 gene silencing (sh-SLC38A5) lentivirus, whereas the control group was transfected with empty vectors (sh-NC and NC). Detailed sequences and vector information for all constructs are provided in **Supplementary Table 1**. Transfection was performed using Lipofectamine™ 3000 (Invitrogen, L3000015, Waltham, MA, USA) reagent. For transfection, a 2 µL aliquot of the viral solution (1×10^9 PFU/mL) was added to each well.

To verify the regulation of SLC38A5 on the mTOR pathway, stable SLC38A5-knockdown cells were treated with MHY1485 (5 µM; Selleck, S7811, Houston, TX, USA), a concentration selected based on previous reports [16], for 24 hours. Control groups received equivalent Dimethyl Sulfoxide (DMSO, Sigma-Aldrich, D8418, St. Louis, MO, USA).

Cell Proliferation Assay

Cell proliferation was evaluated utilizing a CCK-8 kit (Yeasen, 40203ES60, Shanghai, China). Cells were cultured in 96 well plates at a density of 1×10^4 per well. Following the manufacturer's instructions, 20 µL of CCK-8 solution was added to each well, and the plate was incubated in the dark for two hours. Absorbance was measured at 450 nm using a spectrophotometer (Thermo Fisher Scientific, Multiskan FC, Waltham, MA, USA). Cell viability was calculated as follows: (OD_{450} experimental group - OD_{450} blank group)/ (OD_{450} control group - OD_{450} blank group) × 100%.

The cell proliferation ability was further assessed using the BeyoClick™ EdU-594 kit (Beyotime, C0078S, Shanghai, China). Cells were seeded in 48 well plates at a density of 5×10^4 per well and cultured overnight. For cell labeling, a 20 µM EdU working solution was introduced into each well. After fixation and permeabilization, 0.5 mL Click reaction solution was added, followed by five minutes of DAPI (Solarbio, C0065, Beijing, China) staining in the dark. After mounting with an antifade reagent, images were acquired using fluorescence microscopy (Keyence, BZ-X800, Osaka, Japan) for subsequent quantification. The EdU-positive rate was quantified as the percentage of EdU-positive cells (green) relative to the total number of DAPI-stained nuclei (blue) in multiple random fields using ImageJ software (Version 1.48, National Institutes of Health, Bethesda, MD, USA).

Cell Migration and Invasion Assay

Cells were seeded in six well plates (2×10^5 cells/well) and cultured to confluence. A scratch was made in the monolayer using a 200 µL sterile pipette tip. The scratch healing was observed under a microscope (0 hours and 24 hours) (Keyence, BZ-X800, Osaka, Japan). The wound healing rate was calculated as follows: (1 - scratched area at 24 hours/scratched area at 0 hours) × 100%.

Cells were seeded in the Matrigel (BD Biosciences, 356234, Tewksbury, MA, USA)-coated upper chambers of 24-well plates at a density of 1×10^5 per chamber. After 24 hours of culture, the cells under the membrane were stained with crystal violet (Servicebio, G1014, Wuhan, China) and counted under a microscope (Keyence, BZ-X800, Osaka, Japan). The total invasion was quantified and expressed as the number of invaded cells per field.

Flow Cytometry

Cell apoptosis and cell cycle were determined using the Annexin V-FITC/PI apoptosis detection kit (Servicebio, G1511) and the cell cycle analysis kit (Beyotime, C1052). Y79 and WERI-Rb1 cells of different groups were seeded in six well plates at a density of 2×10^5 per well, and stained according to the manufacturer's instructions. Flow cytometry was performed using an Agilent flow cytometer (RMNNC-3000, Santa Clara, CA, USA). The instrument settings were as follows: for Annexin V-FITC, excitation at 488 nm and emission detection at 530/30 nm (FL1 channel); for PI in apoptosis, excitation at 488 nm and emission detection at 585/42 nm (FL2 channel); for PI in cell cycle, excitation at 488 nm and emission detection at 617 nm (FL2 or FL3 channel). The acquired data were analyzed employing FlowJo software (Version 10.8.0, FlowJo LLC, Ashland, OR, USA).

MitoTracker Red CMXRos Staining

Mitochondrial function was assessed using the MitoTracker Red CMXRos staining kit (Beyotime, C1049B). Cells were seeded in 48 well plates at a density of 5×10^4 per well. Following incubation with 0.2 µM Mito-

Tracker Red CMXRos for 15–30 minutes, the cells were counterstained with Hoechst 33258 (Beyotime, C1017) for nuclear staining. Fluorescence microscopy (Keyence, BZ-X800, Osaka, Japan) was used to observe mitochondrial morphology and function. The mean fluorescence intensity (MFI) per cell was quantified using ImageJ software (Version 1.48, National Institutes of Health, Bethesda, MD, USA) from multiple random fields per sample.

Mitochondrial Membrane Potential (MMP), Mitochondrial Reactive Oxygen Species (MitoROS), and Mitochondrial Adenosine Triphosphate (ATP) Measurement

MMP was detected using the JC-1 MMP Detection Kit (Beyotime, C2006). The pretreated cells, which were seeded in six well plates at a density of 2×10^5 per well, were co-incubated with JC-1 staining solution for 20 minutes, and fluorescence was analyzed using flow cytometry (Agilent, RMNNC-3000, Santa Clara, CA, USA). The MMP was quantified as the ratio of the cell population in the second quadrant (Q2, JC-1 aggregates, high MMP) to that in the fourth quadrant (Q4, JC-1 monomers, low MMP), expressed as the Q2/Q4 ratio.

MitoROS levels were detected using the Mitochondrial Superoxide Detection Kit (Beyotime, S0061S). Cells were plated in 48 well dishes at a density of 5×10^4 per well and cultured for 24 hours. MitoSOX Red staining solution was prepared according to the instructions, and 1 mL was added to each well for 30 minutes at 37 °C. Afterward, 200 µL Hoechst 33258 staining solution (Beyotime, C1017) was added for 10 minutes in the dark. Fluorescence microscopy (Keyence, BZ-X800, Osaka, Japan) was used to observe and capture images. The MFI of MitoSOX Red (red fluorescence) was quantified using ImageJ software (Version 1.48, National Institutes of Health, Bethesda, MD, USA).

ATP levels were detected using an ATP Assay Kit (Solarbio, BC0300). The pretreated cells were seeded in six well plates at a density of 2×10^5 per well, and after cell lysis with lysis buffer, the cells were centrifuged at 12,000 g for five minutes at 4 °C to collect the supernatant. According to the manufacturer's instructions, the final absorbance was read at 340 nm on a UV spectrophotometer (Shimadzu, UV-2600, Kyoto, Japan). The ATP content was calculated as follows: ATP content ($\mu mol/10^6$ cells) = $[\Delta A_{sample} \div (\Delta A_{standard} \div C_{standard})] \times V_{extraction} \div 5 = 0.125 \times \Delta A_{sample} \div \Delta A\_standard$, where ΔA represents the absorbance value, $C_{standard}$ is the concentration of the provided ATP standard, and $V_{extraction}$ is the volume of the extraction buffer.

Oxygen Consumption Rate (OCR)

The OCR was quantified using the Seahorse XF Cell Mitochondrial Stress Test Kit (Agilent, 103015-100). First, the target cells were seeded in Seahorse XF culture plates at a density of 1×10^4 to 3×10^4 cells per well. Before measurement, the cells were hydrated for 45–60 minutes in a CO_2-free cell incubator (Thermo Scientific, 311, Waltham, MA, USA). The culture plate was then placed in the Seahorse XF analyzer (Agilent, Seahorse XF Pro, Santa Clara, CA, USA), and OCR measurements were performed according to the preset program, recording the oxygen consumption of cells under different treatments. After data collection, the results were processed using Seahorse XF software (Version 2.6.8, Agilent, Santa Clara, CA, USA), and OCR curves were plotted.

qRT-PCR

Following RNA extraction with TRIzol reagent (Servicebio, G3013), cDNA was generated using the PrimeScript™ RT Reagent Kit (Takara, RR037Q, Kusatsu, Shiga, Japan). qPCR was then performed using TB Green® Premix Ex Taq™ II (Takara, RR820Q) on a PCR instrument (Hongshi, SLAN-96S, Shanghai, China). The thermal cycling conditions were as follows: initial denaturation at 95 °C for three minutes, followed by 40 cycles of denaturation at 95 °C for 15 seconds and annealing/extension at 60 °C for 20 seconds. Relative transcript levels were determined by the $2^{-\Delta\Delta CT}$ method using *GAPDH* for normalization, with corresponding primers detailed in Table 1. All primers used were human-specific, as the xenograft tumors were derived from human retinoblastoma cell lines.

Hematoxylin and Eosin (H&E) Staining

After routine dewaxing and rehydration, tissue sections were stained with Hematoxylin (Servicebio, G1004) and Eosin (Servicebio, G1001). After staining, the sections were cleared with eco-friendly transparentizing liquid (Servicebio, G1128). After mounting, histological changes were observed under a microscope (Leica, DM500, Wetzlar, Hesse, Germany).

Immunofluorescence (IF)

After culturing the cells on slides in 48 well plates at a density of 5×10^4 per well, they were fixed and permeabilized. Then, 200 µL of SLC38A5 primary antibody (1:200 dilution, CSB-PA837853LA01HU, Huamei Bio, Wuhan, China) was applied, and the slides were incubated overnight at 4 °C. Afterward, the slides were incubated with 1:300 diluted Cy3-conjugated goat anti-rabbit IgG (H+L) secondary antibody (1:200 dilution, A0516, Beyotime) at 37 °C for one hour. Nuclear staining was performed using DAPI (Solarbio, C0065), and the samples were visualized and images were acquired using a fluorescence microscope (Keyence, BZ-X800, Osaka, Japan). The MFI of SLC38A5 in individual cells was quantified using ImageJ software (Version 1.48, National Institutes of Health, Bethesda, MD, USA).

Table 1. Primers used in qRT-PCR.

Gene	Forward sequence (5′-3′)	Reverse sequence (5′-3′)
GAPDH (Human)	GCACCGTCAAGGCTGAGAAC	TGGTGAAGACGCCAGTGGA
SLC38A5 (Human)	GCTACAGGCAAGAACGTGAGG	ATTCCAAACGATGTCTTCCCC
Ki67 (Human)	ACGCCTGGTTACTATCAAAAGG	CAGACCCATTTACTTGTGTTGGA
PCNA (Human)	CCTGCTGGGATATTAGCTCCA	CAGCGGTAGGTGTCGAAGC

GAPDH, Glyceraldehyde-3-phosphate dehydrogenase; *SLC38A5*, Solute Carrier Family 38 Member 5; *Ki67*, Kiel67; *PCNA*, proliferating cell nuclear antigen.

Immunohistochemistry (IHC)

The universal immunohistochemistry kit (Zsbio, PV-6000, Beijing, China) was employed for antigen detection. Following deparaffinization and rehydration, the tissue sections underwent antigen retrieval and were treated with an endogenous peroxidase blocking solution. Then, the sections were incubated overnight at 4 °C with anti-SLC38A5 antibody (1:200 dilution, Ab72717, Abcam, Cambridge, MA, USA) and anti-Ki67 antibody (1:100 dilution, 28074-1-AP, Proteintech, Wuhan, China). Afterward, the sections were incubated with 100 µL of enzyme-labeled goat anti-mouse/rabbit IgG polymer at 37 °C for 20 minutes. Finally, the sections were developed with DAB (Servicebio, G1212) and counterstained with Hematoxylin (Servicebio, G1005-1). Histological sections were examined under a light microscope (Leica, DM500, Wetzlar, Hesse, Germany). The staining intensity of SLC38A5 and Ki67 was semi-quantitatively assessed using ImageJ software (Version 1.48, National Institutes of Health, Bethesda, MD, USA) based on the MFI from multiple random fields.

Western Blotting (WB)

Following protein extraction with RIPA buffer (Bio Sharp, BL504A, Hefei, China) and concentration determination via the BCA kit (Bio Sharp, BL521A). Equal protein aliquots were subjected to SDS-PAGE, transferred to membranes, and blocked for two hours. Membranes were then probed overnight at 4 °C with the following primary antibodies: SLC38A5 (Abcam, ab72717), Ki67 (Abcam, ab16667), PCNA (Abways, AB0051, Shanghai, China), mTOR (Abcam, ab109268), GAPDH (Abcam, ab8245), and p-mTOR (Proteintech, 67778-1-Ig), all diluted at 1:1000. After washing, HRP-conjugated secondary antibodies were incubated at 37 °C for two hours. The secondary antibodies used were ab6789 for p-mTOR and GAPDH, and ab6721 for all other target proteins (both diluted at 1:5000, Abcam). Finally, the blots were developed using Immobilon Western chemiluminescent HRP substrate (Millipore, WBKLS0100, Burlington, MA, USA), and the chemiluminescent signals were captured on a gel imaging system (SINSAGE, ChampChemi 910, Beijing, China). The protein expression levels were normalized to the internal control GAPDH to account for variations in sample loading.

Xenograft Experiment

Twenty-four male BALB/c-nu nude mice (6–8 weeks, 18–22 g) were obtained from Beijing SPF Biotechnology (China). The mice were housed in an SPF animal lab at 21–23 °C, 60–65% humidity for one week with free access to food and water. After adaptation, two independent xenograft experiments were conducted, each with its own randomization procedure. Mice were randomly assigned to groups (n = 6) as follows: WERI-Rb1 cells: NC, SLC38A5-OE; Y79 cells: sh-NC, sh-SLC38A5. Randomization for each experiment was performed separately by generating a random number for each mouse using the RAND() function in Excel, sorting mice in ascending order based on these numbers, and then sequentially allocating them to the respective groups within that experiment. This allocation was performed by a researcher not involved in subsequent experiments to maintain allocation concealment.

To establish xenografts, 5×10^6 WERI-Rb1 cells overexpressing SLC38A5 and 5×10^6 Y79 cells with SLC38A5 knockdown were subcutaneously injected into the dorsal flanks of mice. Tumor volumes were measured weekly starting from Day 7 using calipers and calculated using the formula: $V = (L \times W^2)/2$ (L = tumor length, W = width). On Day 26, mice were euthanized by CO_2 inhalation. Specifically, mice were placed individually in a euthanasia chamber, and 100% CO_2 was introduced at a fill rate of 30–70% of the chamber volume per minute for five minutes. Thereafter, cervical dislocation was performed, and the absence of heartbeat and respiration was confirmed. Subcutaneous tumors were removed, photographed, weighed, and growth curves plotted. All procedures were conducted with the approval of the Ethics Committee guidelines and animal ethics standards of Sheng' ers Biology (No: SES-IACUC-25-005).

Statistical Analysis

All experimental data are derived from independent biological replicates. For *in vitro* experiments, n = 3 represents three independent biological replicates, each performed with separately cultured cells. The number of replicates (n = 6) in *in vivo* animal experiments refers to the number of independent mice per experimental group. For comparisons among three or more groups, one-way ANOVA was performed. When the overall ANOVA indicated a significant difference, Tukey's honest significant difference

(HSD) post hoc test was applied to control the family-wise error rate while comparing all possible pairs of group means. Statistical differences between two groups were assessed using Student's *t*-test. For key experiments, effect sizes (partial η^2 for one-way ANOVA) were reported alongside *p* values. $p < 0.05$ was considered statistically significant. All statistical analysis was performed using GraphPad Prism 9.5 (Version 9.5, GraphPad Software, San Diego, CA, USA).

Results

Inhibition of SLC38A5 Expression Weakens the Biological Functions of Human RB Cells

qRT-PCR (Fig. 1A) and WB (Fig. 1B) analysis showed that SLC38A5 expression was significantly upregulated in human RB cell lines (WERI-Rb1, Y79, SO-Rb50), with notably higher expression in Y79 and WERI-Rb1 cells ($p < 0.01$). To study the role of SLC38A5 in cellular function, we knocked down SLC38A5 in Y79 cells. Among the two sequences, sh-SLC38A5-1 was selected for all subsequent experiments because of its superior knockdown efficiency (**Supplementary Fig. 1A,B**) ($p < 0.05$). WB (Fig. 1C) and qRT-PCR (**Supplementary Fig. 1C**) detection showed that SLC38A5 knockdown significantly reduced the expression of proliferation markers Ki67 and PCNA ($p < 0.01$). CCK-8 (Fig. 1D) results showed that cell viability was significantly decreased in the sh-SLC38A5 group at 24, 48, and 72 hours ($p < 0.05$). EdU (Fig. 1E,F) results similarly showed that SLC38A5 knockdown inhibited cell proliferation ($p < 0.01$). Scratch assay (Fig. 1G,H) and Transwell assay (Fig. 1I,J) collectively demonstrated that SLC38A5 knockdown significantly inhibited cell migration and invasion ($p < 0.01$). Flow cytometry analysis (Fig. 1K) indicated that SLC38A5 knockdown increased the apoptosis rate and caused a G1 phase cell cycle arrest, with a decrease in the number of cells in G2 phases, whereas the S phase fraction showed no significant alteration (Fig. 1L) ($p < 0.01$).

SLC38A5 Overexpression Enhances the Biological Functions of Human RB Cells

To assess the functional consequences of SLC38A5 upregulation, SLC38A5 was overexpressed in the WERI-Rb1 cells. Transcript and protein analysis demonstrated that the SLC38A5 expression in the SLC38A5-OE group was significantly increased, along with concomitant upregulation of Ki67 and PCNA (Fig. 2A,B) ($p < 0.01$). Functionally, SLC38A5 overexpression enhanced cell viability, proliferation, migration, and invasion while reducing apoptosis (Fig. 2C–J) ($p < 0.01$). Cell cycle analysis further showed a shift with decreased G1 and increased S/G2 phases (Fig. 2K) ($p < 0.05$).

SLC38A5 Overexpression and Knockdown Affect Mitochondrial Function in WERI-Rb1 and Y79 Cells

To assess the effects of SLC38A5 on mitochondrial function, SLC38A5 was knocked down in Y79 cells and overexpressed in WERI-Rb1 cells, followed by various assays. MitoTracker Red staining (Fig. 3A) ($p < 0.001$) and JC-1 flow cytometry (Fig. 3B) ($p < 0.001$) consistently demonstrated that SLC38A5 overexpression in WERI-Rb1 cells significantly enhanced MMP, whereas knockdown in Y79 cells markedly reduced it. ATP production and OCR measurements revealed that SLC38A5 overexpression significantly boosted ATP generation, along with a substantial increase in both Basal OCR and Maximal OCR, whereas SLC38A5 knockdown had the opposite effect (Fig. 3C,D) ($p < 0.05$). Quantitative analysis of MitoSOX staining further showed that SLC38A5 overexpression markedly increased superoxide levels, with a significant rise in red fluorescence, whereas SLC38A5 knockdown reversed this effect (Fig. 3E) ($p < 0.01$).

SLC38A5 Regulates Mitochondrial Function in Y79 Cells via the mTOR Pathway

The regulatory influence of SLC38A5 on the mTOR pathway and mitochondrial function was thoroughly assessed. WB analysis (Fig. 4A,B) revealed that in Y79 cells, SLC38A5 knockdown significantly decreased the p-mTOR/mTOR ratio, whereas SLC38A5 overexpression in WERI-Rb1 cells produced the opposite trend ($p < 0.001$). Quantitative analysis of MitoTracker Red staining (Fig. 4C) showed a marked reduction in red fluorescence in the SLC38A5 knockdown group, which was reversed by treatment with the activator MHY1485 ($p < 0.01$). Further JC-1 staining analysis (Fig. 4D) demonstrated that the red/green fluorescence ratio in the M2 (sh-SLC38A5) group was significantly decreased, whereas the M4 (sh-SLC38A5+MHY1485) group exhibited the opposite result ($p < 0.05$). ATP assays (Fig. 4E) showed that SLC38A5 knockdown significantly reduced ATP production, whereas MHY1485 treatment notably reversed this effect ($p < 0.01$). Real-time OCR profiling (Fig. 4F) further demonstrated that MHY1485 treatment can reverse impaired mitochondrial function. Quantitative analysis (Fig. 4G) confirmed that MHY1485 restoration recovered respiratory capacity to near-normal levels ($p < 0.01$). Finally, MitoSOX staining and subsequent quantification (Fig. 4H,I) demonstrated that the level of intracellular superoxide anions was significantly elevated in the M4 group ($p < 0.001$).

SLC38A5 Regulates the Biological Functions of Y79 Cells via the mTOR Pathway

The experimental results showed that in the SLC38A5 knockdown (M2) group, both the mRNA and protein expression of SLC38A5, Ki67, and PCNA were significantly reduced. However, treatment with MHY1485 (M4 group) rescued Ki67 and PCNA expression ($p < 0.05$), whereas

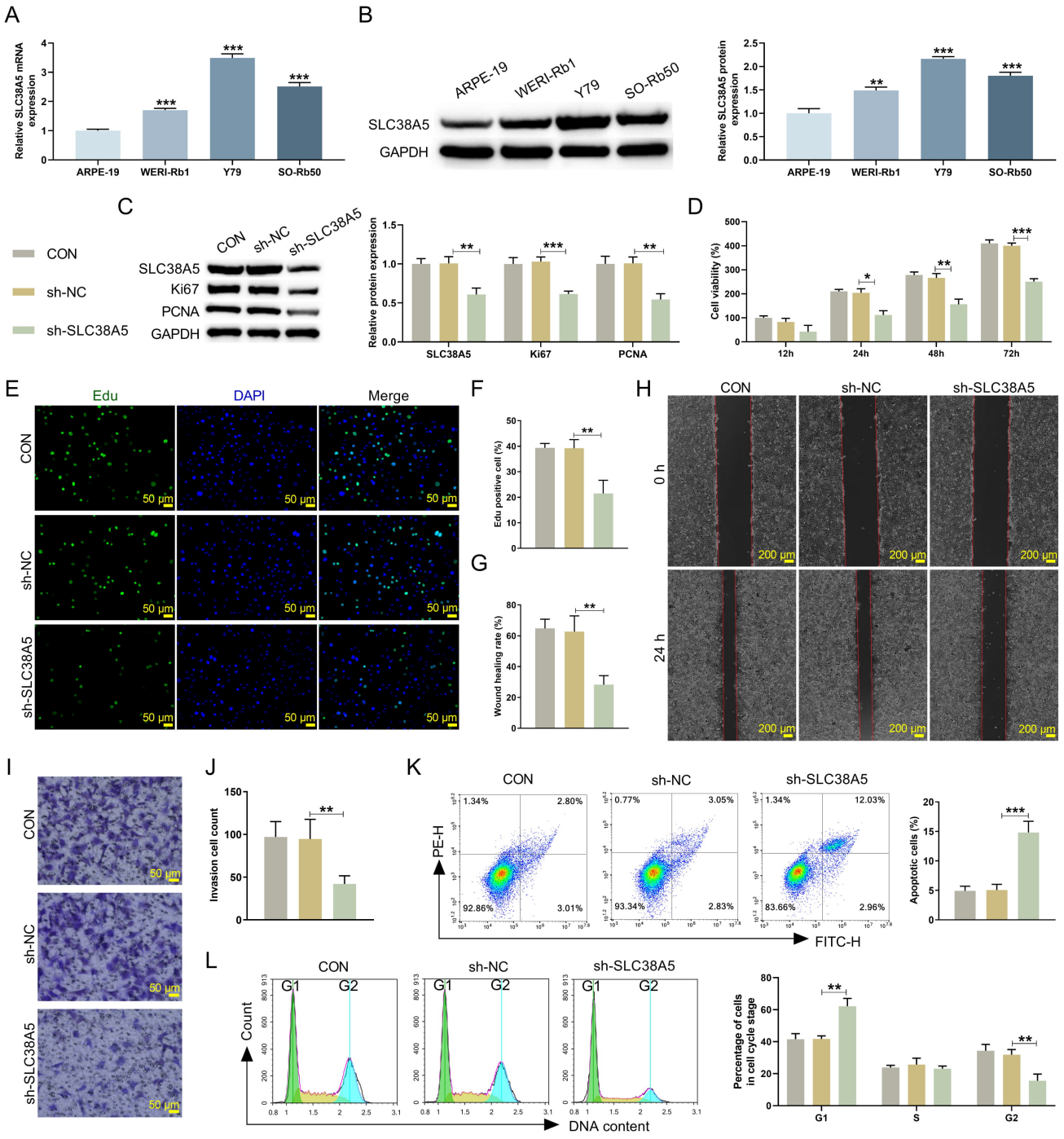

Fig. 1. The effect of SLC38A5 knockdown on the proliferation, migration, invasion, and apoptosis of Y79 cells. (A,B) qRT-PCR and WB were conducted to measure the expression level of SLC38A5 in different cell lines (ARPE-19, WERI-Rb1, Y79, SO-Rb50) (n = 3). Experimental groups: CON, sh-NC, sh-SLC38A5. (C) WB analysis of SLC38A5, Ki67, and PCNA expression (n = 3). (D) The CCK-8 assay was employed to determine the cell viability (n = 3). (E,F) The EdU assay was utilized to examine cell proliferation rates (n = 3). (G,H) Scratch assay was used to assess cell migration ability at 0 hours and 24 hours (n = 3). (I,J) The Transwell assay demonstrated the cell invasion ability (n = 3). (K,L) Flow cytometry was used to examine the apoptotic cell distribution and cell cycle phase percentages (n = 3). All of the above experiments were biological replicates. *$p < 0.05$, **$p < 0.01$, ***$p < 0.001$ vs ARPE-19/sh-NC group (designated control for knockdown experiments). SLC38A5, Solute Carrier Family 38 Member 5; qRT-PCR, quantitative real-time polymerase chain reaction; WB, Western blotting; ARPE-19, adult retinal pigment epithelium cell line-19; WERI-Rb1, WERI retinoblastoma 1; Y79, human retinoblastoma cell line Y79; SO-Rb50, SO retinoblastoma 50; CON, control; sh-NC, short hairpin RNA negative control; Ki67, Kiel67; PCNA, proliferating cell nuclear antigen; CCK-8, cell counting kit-8; EdU, 5-ethynyl-2′-deoxyuridine.

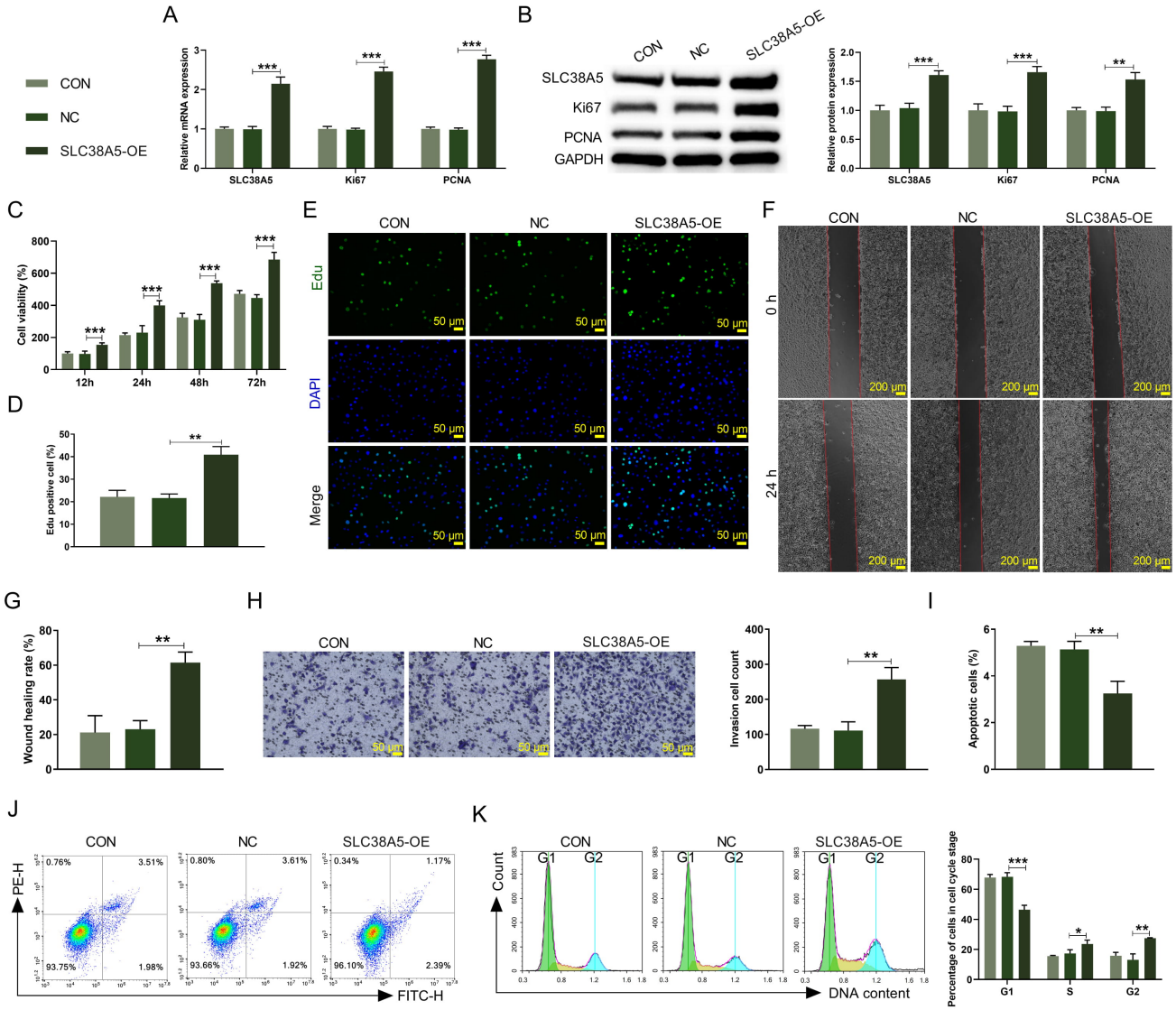

Fig. 2. The effect of SLC38A5 overexpression on the biological functions of WERI-Rb1 cells. *In vitro* experimental groups: CON, sh-NC, sh-SLC38A5. (A,B) qRT-PCR and WB were performed to measure the expression levels of SLC38A5, Ki67, and PCNA (n = 3). (C) CCK-8 assay was conducted to assess cell viability (n = 3). (D,E) EdU assay was used to evaluate cell proliferation (n = 3). (F,G) Scratch assay showed cell migration at 0 hours and 24 hours (n = 3). (H) Transwell assay was employed to detect the cell invasion ability (n = 3). (I–K) Flow cytometry was utilized to evaluate the cell apoptosis rate and cell cycle distribution (n = 3). All of the above experiments were biological replicates. *$p < 0.05$, **$p < 0.01$, ***$p < 0.001$, vs NC group (designated control for overexpression experiments).

SLC38A5 expression remained unchanged (Fig. 5A,B). Further analysis with CCK-8 (Fig. 5C) and EdU staining assays (Fig. 5D,E) revealed a significant decrease in cell proliferation in the M2 group, whereas MHY1485 treatment restored proliferative capacity ($p < 0.01$). Scratch (Fig. 5F,G) and Transwell assays (Fig. 5H,I) demonstrated that SLC38A5 silencing inhibited cell migration and invasion, and MHY1485 treatment significantly ameliorated these effects ($p < 0.05$). Flow cytometry analysis further showed that MHY1485 treatment significantly reduced apoptosis rates and led to a marked decrease in the proportion of cells in the G1 phase and an increase in the proportion of cells in the G2 phase (Fig. 5J–M) ($p < 0.01$). In summary, SLC38A5 plays a crucial role in the malignant behaviors of RB cells, and MHY1485 treatment can partially reverse these alterations.

High Expression of SLC38A5 Promotes Tumor Growth, Whereas Low Expression Inhibits Tumor Progression in Xenograft Models

SLC38A5 plays a critical role in regulating tumor cell proliferation and growth. Two independent *in vivo* experiments were conducted. In the WERI-Rb1 model, SLC38A5 overexpression significantly elevated the expres-

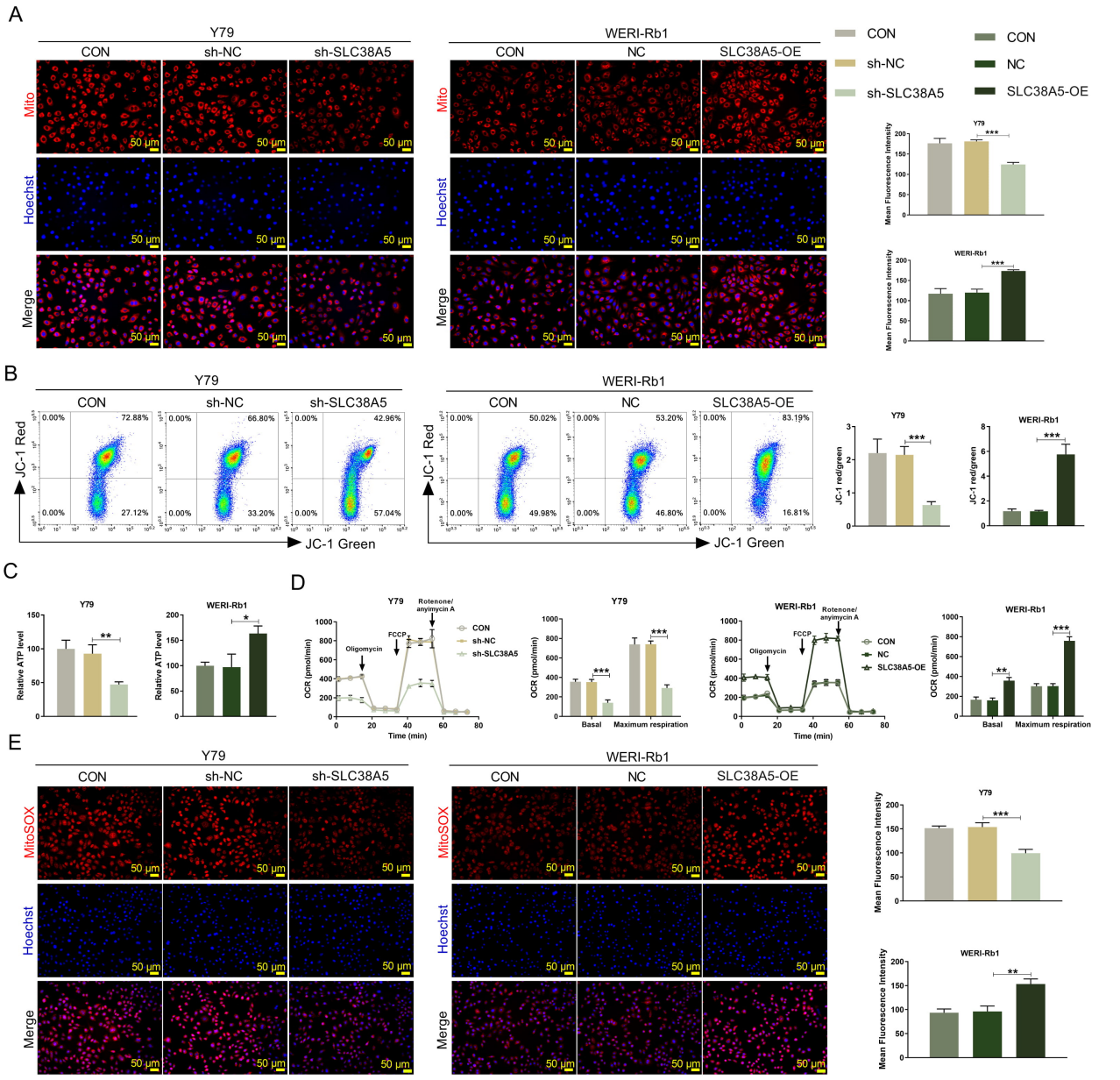

Fig. 3. Regulation of mitochondrial function by SLC38A5 overexpression and knockdown in WERI-Rb1 and Y79 cells. Experimental Groups: Y79: CON, sh-NC, sh-SLC38A5; WERI-Rb1: CON, NC, SLC38A5-OE. (A) MitoTracker Red staining was used to observe mitochondrial morphology (n = 3). (B) Flow cytometry analysis of MMP using JC-1 staining (n = 3). (C) ATP levels were measured using an ATP kit (n = 3). (D) OCR measurements showing basal respiration and maximal respiration (n = 3). (E) MitoSOX Red staining was used to detect mitochondrial superoxide levels (n = 3). All of the above experiments were biological replicates. *$p < 0.05$, **$p < 0.01$, ***$p < 0.001$, vs sh-NC group (designated control for knockdown experiments) or NC group (designated control for overexpression experiments). MMP, Mitochondrial Membrane Potential; JC-1, 5,5′,6,6′-tetrachloro-1,1′,3,3′-tetraethylbenzimidazolylcarbocyanine iodide; ATP, Adenosine Triphosphate; OCR, Oxygen Consumption Rate.

sion of SLC38A5, Ki67, and PCNA compared to its NC control (Fig. 6A–C) ($p < 0.05$). H&E staining (Fig. 6E) further revealed proliferative histopathology. Accordingly, tumor volume (Fig. 6F), visual size (Fig. 6G), and tumor weight (Fig. 6H) were all significantly greater in the SLC38A5-OE group ($p < 0.01$). Conversely, in the separate Y79 model, SLC38A5 silencing substantially decreased the expression of the same markers, induced inhibitory histopathology with necrosis, and significantly suppressed tumor volume, visual size, and weight compared to its sh-NC control (Fig. 6A–H) ($p < 0.01$). These parallel yet independent results consistently underscore the critical role of SLC38A5 in promoting tumor proliferation and growth.

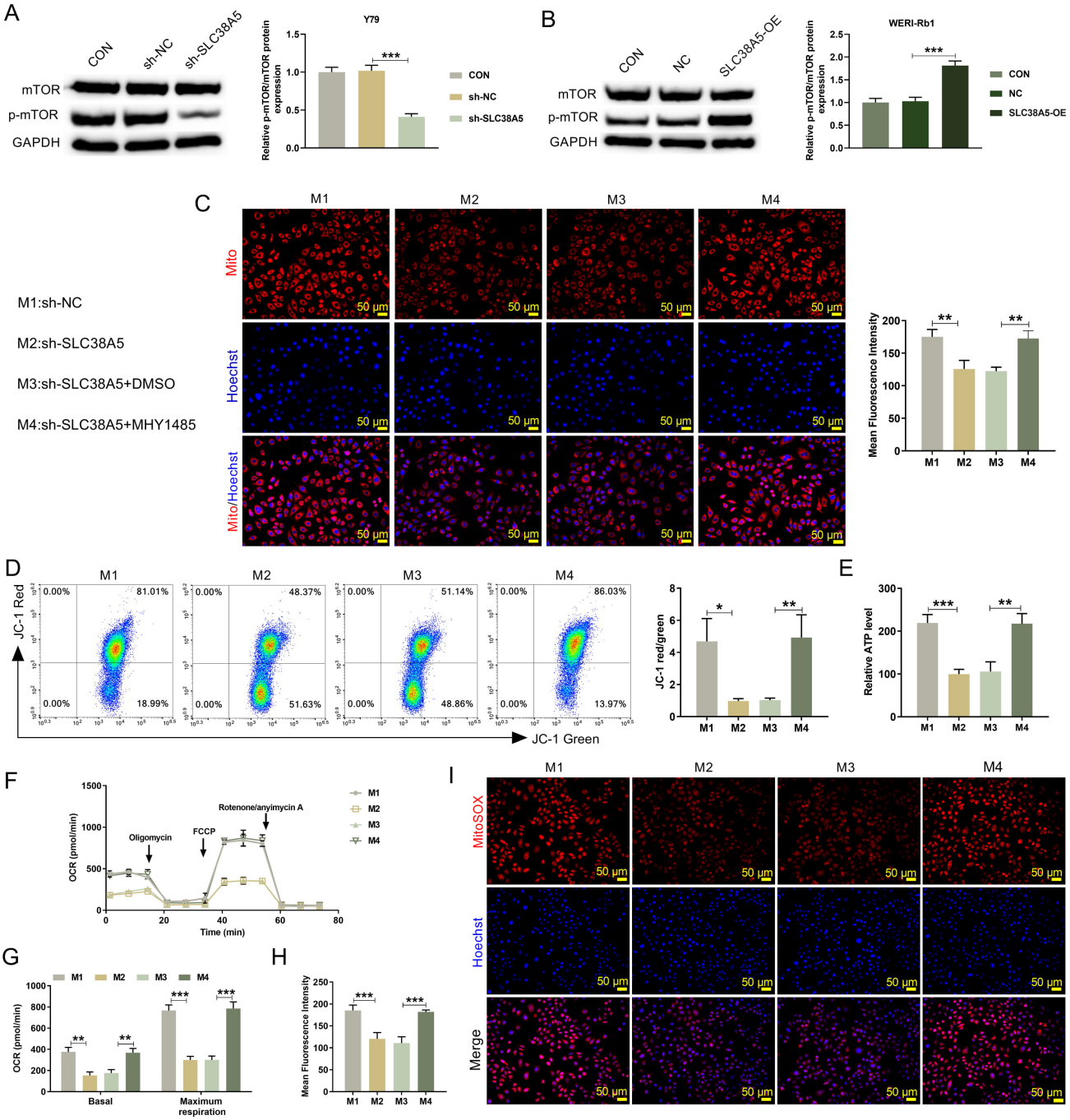

Fig. 4. SLC38A5 knockdown regulates mitochondrial function in Y79 cells by inhibiting the mTOR pathway. (A,B) WB was carried out to quantify the protein levels of p-mTOR/mTOR in Y79 cells or WERI-Rb1 cells (n = 3). (C) MitoTracker Red staining was used to detect MMP in Y79 cells (n = 3). (D) JC-1 staining followed by flow cytometric analysis was performed to evaluate MMP in Y79 cells (n = 3). (E) ATP levels were measured in Y79 cells using an ATP kit (n = 3). (F,G) OCR analysis was performed on Y79 cells, and the results were visualized (n = 3). (H,I) Mitochondrial superoxide levels were evaluated in Y79 cells using MitoSOX Red staining (n = 3). All of the above experiments were biological replicates. *$p < 0.05$, **$p < 0.01$, ***$p < 0.001$, vs sh-NC group (designated control for knockdown experiments), NC group (designated control for overexpression experiments), M1 group (designated control for knockdown experiments), or M3 group (designated knockdown control with vehicle treatment). mTOR, mechanistic target of rapamycin.

Discussion

RB is a predominant childhood ocular malignancy, characterized by high invasiveness and the threat it poses to vision and life [17,18]. Despite recent progress in the diagnosis and treatment of RB, its precise pathogenesis remains unclear, and the identification of effective molecu-

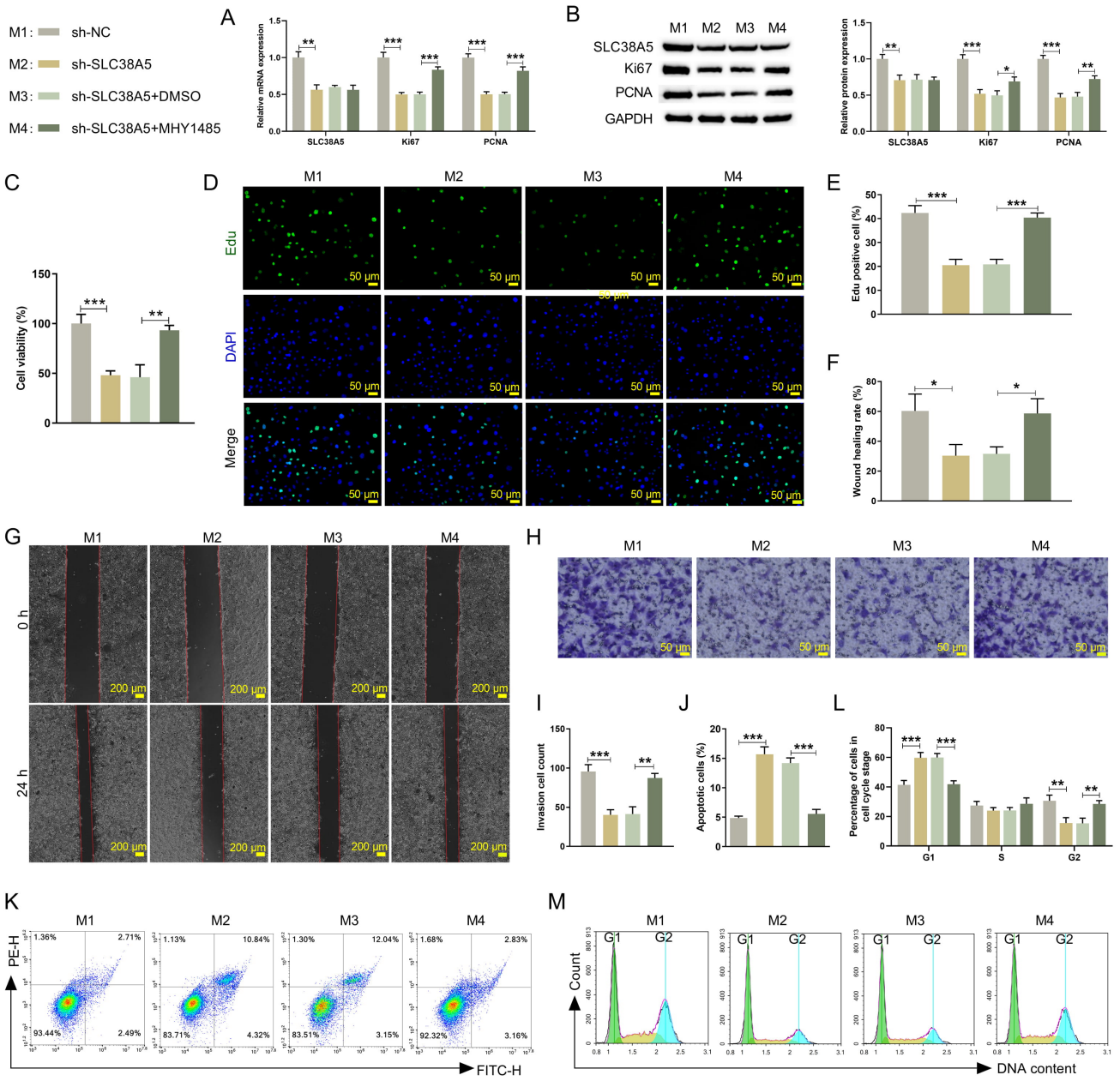

Fig. 5. SLC38A5 knockdown regulates Y79 cell proliferation, migration, invasion, and apoptosis by inhibiting the mTOR pathway. (A,B) qRT-PCR and WB analysis were performed to measure the expression levels of SLC38A5, Ki67, and PCNA (n = 3). (C–E) Cell proliferation activity was analyzed using CCK-8 and EdU assay (n = 3). (F,G) Scratch assay showed cell migration at 0 hours and 24 hours (n = 3). (H,I) The Transwell assay was conducted to evaluate cell invasion ability (n = 3). (J,K) The percentage of apoptotic cells and cell cycle distribution was assessed by flow cytometry (n = 3). (L,M) Flow cytometry was employed to evaluate the cell cycle distribution (n = 3). All of the above experiments were biological replicates. $*p < 0.05$, $**p < 0.01$, $***p < 0.001$, vs M1 group (designated control for knockdown experiments) or M3 group (designated knockdown control with vehicle treatment).

lar therapeutic targets remains challenging [19–21]. Therefore, a deeper mechanistic understanding of RB pathogenesis is crucial for developing more effective treatment strategies.

SLC38A5 has gained increasing attention for its role in tumor cells in recent years. Amino acid transporters are not only essential for maintaining cellular metabolic balance and energy supply, but they also regulate cell proliferation and survival through signaling pathways [22]. A study has shown that inhibiting the function and expression of SLC38A5 disrupts glutamine metabolism, thereby suppressing TNBC cell function [15]. In colorectal cancer (CRC), SLC38A5 deficiency inhibits the proliferation, migration, and invasion of CRC cell lines [23]. In this study, SLC38A5 expression in RB was identified and its pivotal role in modulating tumor cell functions was demonstrated.

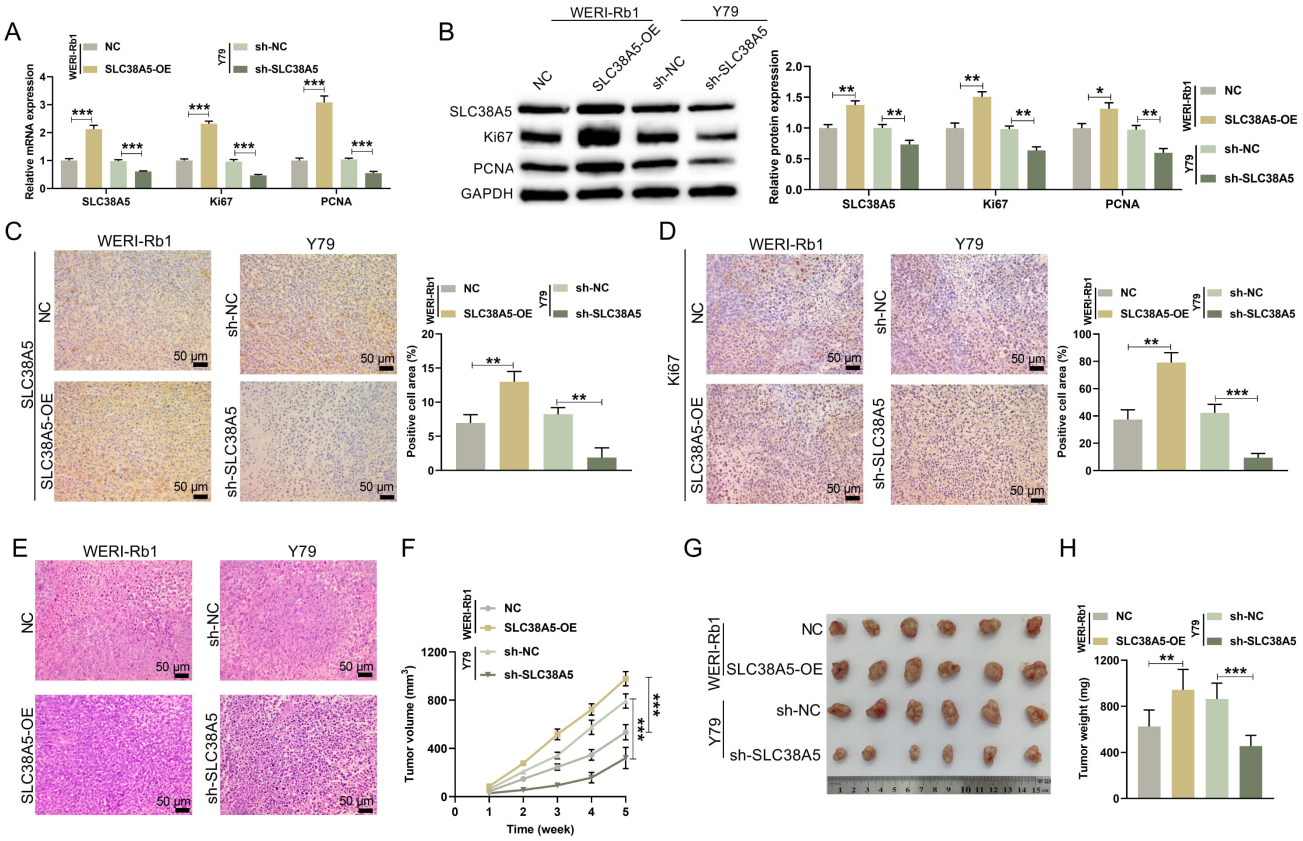

Fig. 6. SLC38A5 overexpression promotes tumor growth, whereas low expression inhibits tumor progression *in vivo*. Experimental groups: WERI-Rb1 xenograft: NC, SLC38A5-OE; Y79 xenograft: sh-NC, sh-SLC38A5. (A,B) qRT-PCR and WB analysis were performed to measure the expression levels of SLC38A5, Ki67, and PCNA (n = 3). (C,D) IHC staining detected SLC38A5 and Ki67 expression (n = 6). (E) Hematoxylin and Eosin (H&E) staining was conducted to examine pathological damage (n = 6). (F) Tumor volume changes were measured at weeks 1–5 (n = 6). (G) Photographic documentation of tumors harvested from nude mice (n = 6). (H) Tumor weight was measured in each group (n = 6). All of the above experiments were biological replicates. Each group in the animal experiments included six mice. $*p < 0.05$, $**p < 0.01$, $***p < 0.001$, vs NC group (designated control for overexpression experiments) or sh-NC group (designated control for knockdown experiments). IHC, Immunohistochemistry.

Further functional experiments confirmed that its knockdown effectively suppressed tumor cell malignancy and induced G1 arrest, whereas overexpression had opposing effects. These results indicated that SLC38A5 participated in the malignant progression of RB by regulating key biological processes in tumor cells.

Additionally, we found that the SLC38A5 overexpression significantly enhanced the mitochondrial metabolic activity of Y79 and WERI-Rb1 cells, including increased MMP, ATP production, and OCR. However, this enhanced mitochondrial activity was accompanied by a significant rise in MitoROS levels, suggesting that it might trigger metabolic stress and lead to mitochondrial dysfunction. Notably, mitochondrial ROS have a dual role in tumor progression, as they can accelerate tumor development by promoting a malignant cellular phenotype, but may also induce cell death [24]. Previous investigations have revealed that MitoROS serve a context-dependent function in tumor progression. In this study, the accumulation of MitoROS induced by SLC38A5 may promote the malignant progression of RB by activating downstream proliferative signaling pathways. This finding underscores the critical role of SLC38A5 in regulating tumor cell metabolism and behavior.

The mTOR signaling pathway, a master regulator of cellular metabolism and growth, is closely associated with tumorigenesis through its abnormal activation [25,26]. Baicalein inhibits the mTOR pathway and triggers programmed cell death in lung cancer cells [27]. Conversely, in breast cancer, SLC38A5 not only stimulates proliferation, but also confers cisplatin resistance by modulating mTOR signaling [28]. This study showed that SLC38A5 knockdown significantly reduced mTOR pathway activity, whereas SLC38A5 overexpression enhanced its activation. Additionally, treatment with the mTOR activator MHY1485 [29] partially reversed the mitochondrial dysfunction caused by SLC38A5 knockdown. This suggested that SLC38A5 might regulate mitochondrial func-

tion through mTOR pathway activation, thereby affecting key oncogenic phenotypes. This discovery not only reveals a new mechanism by which SLC38A5 regulates tumor metabolism, but also provides new insights into the interplay between mTOR signaling and tumor metabolism.

SLC38A5 expression correlates strongly with mTOR pathway activity. SLC38A5 is responsible for the cellular uptake of key amino acids, including glutamine, leucine, and asparagine. These amino acids can activate mTORC1 localization and activation through amino acid-sensing mechanisms involving Rag GTPases [30,31]. In this study, we hypothesize that SLC38A5 may activate the mTOR pathway by modulating intracellular amino acid levels. This hypothesis aligns with the mechanisms by which other amino acid transporters, such as SLC38A9 [32,33], SLC1A5 [34,35], and SLC7A5 [36,37], regulate mTOR activity. Although we did not directly measure intracellular amino acid levels or further delineate the molecular mechanisms, existing literature and our functional data provide compelling support for this hypothesis. Future studies should employ amino acid metabolomics, stable isotope tracing, and assessment of mTOR downstream effector phosphorylation to elucidate the mechanism by which SLC38A5 regulates the mTOR pathway through amino acid metabolism, and to assess its potential application in targeted therapy.

In the *in vivo* xenograft model, SLC38A5 overexpression significantly promoted tumor growth, whereas SLC38A5 knockdown inhibited tumor volume increase and proliferative activity. These *in vivo* outcomes corroborated the *in vitro* data, collectively establishing the essential role of SLC38A5 in tumor cell growth. Additionally, the cell cycle-related proteins Ki67 and PCNA are widely used as markers of cell proliferation, crucial for detecting cell division and proliferative activity [38]. The high expression of Ki67 and PCNA in the SLC38A5 overexpression group suggests the importance of SLC38A5 in regulating tumor cell proliferation. The presence of prominent necrotic areas in tumors from the SLC38A5 silencing group suggests that SLC38A5 may inhibit tumor progression by suppressing tumor cell metabolic activity and survival.

Despite providing valuable insights into the oncogenic functions of SLC38A5 in tumor cells, some limitations should be acknowledged. First, this study was confined to cellular models and did not include clinical patient samples. Future clinical studies are needed to validate these findings and determine their potential clinical significance. The functional alterations of SLC38A5 observed in this study require further validation through clinical investigations to determine its potential clinical relevance. Second, future studies should further expand the understanding of SLC38A5's mechanistic and functional roles in other cancers, especially its interplay with metabolic regulation and signaling networks. Finally, given the close link between SLC38A5 and amino acid metabolism, targeting its metabolic function—through inhibitor development or metabolic intervention—may offer new avenues for precise RB treatment.

Although the subcutaneous xenograft model successfully validated the role of SLC38A5 in promoting tumor growth and activating the mTOR pathway, it fails to recapitulate the unique intraocular microenvironment of retinoblastoma—including the blood-retinal barrier, neuronal-glial interactions, and the distinct metabolic milieu of the vitreous cavity. Therefore, although this study's findings robustly demonstrate that SLC38A5 enhances the intrinsic proliferative capacity of tumor cells, its potential roles in critical clinicopathological processes such as intraocular invasion or optic nerve infiltration, remain unexplored. Future studies should prioritize employing orthotopic intraocular transplantation models or genetically engineered mouse models that spontaneously develop retinoblastoma. These models would enable a more physiologically relevant investigation of SLC38A5 function and provide a more accurate assessment of its therapeutic potential.

Conclusion

In summary, our findings delineate the mechanism by which SLC38A5 promotes RB cell proliferation, migration, and invasion through the mTOR signaling pathway and mitochondrial function. These findings lay the foundation for further research into the mechanisms of SLC38A5 and its potential applications in cancer therapy.

Abbreviations

H&E, Hematoxylin and Eosin; IF, Immunofluorescence; IHC, Immunohistochemistry; MMP, Mitochondrial Membrane Potential; MitoROS, Mitochondrial Reactive Oxygen Species; OCR, Oxygen Consumption Rate; RB, Retinoblastoma; SLC38A5, Solute Carrier Family 38 Member 5; TNBC, Triple-Negative Breast Cancer.

Availability of Data and Materials

All data generated and/or analyzed during the current study are available from the corresponding author on reasonable request.

Author Contributions

CW: Conceptualization, Data curation, Formal analysis, Investigation, Writing-original draft, Writing-review & editing. YD: Conceptualization, Data curation, Formal analysis, Writing-original draft, Writing-review & editing. XX: Formal analysis, Methodology, Writing-review & editing. YL: Software, Validation, Writing-review & editing. XY: Conceptualization, Project administration, Resources, Supervision, Writing-review & editing. All authors gave fi-

nal approval of the version to be published. All authors have participated sufficiently in the work to take public responsibility for appropriate portions of the content and agreed to be accountable for all aspects of the work in ensuring that questions related to its accuracy or integrity.

Ethics Approval and Consent to Participate

All procedures were conducted with the approval of the Ethics Committee guidelines and animal ethics standards of Sheng' ers Biology (No: SES-IACUC-25-005). All animal experimental methods are reported in accordance with ARRIVE guidelines for the reporting of animal experiments.

Acknowledgment

Not applicable.

Funding

This research received no external funding.

Conflict of Interest

The authors declare no conflict of interest.

Supplementary Material

Supplementary material associated with this article can be found, in the online version, at https://doi.org/10.24976/Discov.Med.202638205.41.

References

[1] Kiosis G, Skourtsidis K, Ioannou D, Tseriotis VS, Stergiou K, Akritidou F, *et al*. Epigenetic Factors in Pathogenesis of Retinoblastoma: DNA Methylation and Histone Acetylation. Current Issues in Molecular Biology. 2025; 47: 844. https://doi.org/10.3390/cimb47100844.

[2] Pareek A, Kumar D, Pareek A, Gupta MM, Jeandet P, Ratan Y, *et al*. Retinoblastoma: An update on genetic origin, classification, conventional to next-generation treatment strategies. Heliyon. 2024; 10: e32844. https://doi.org/10.1016/j.heliyon.2024.e32844.

[3] Feng Y, Feng X, Lv Y. Worldwide Burden of Retinoblastoma from 1990 to 2021. Ophthalmic Research. 2024; 67: 672–682. https://doi.org/10.1159/000542193.

[4] Chen J, Cao X, Xu S, Chen X, Xie R, Ye G, *et al*. Global, regional, and national burden of retinoblastoma in infants and young children: findings from the global burden of disease study 1990-2021. EClinicalMedicine. 2024; 76: 102860. https://doi.org/10.1016/j.eclinm.2024.102860.

[5] Zhang Y, Wang Y, Zhi T, Jin M, Huang D, Ma X. Clinical characteristics, treatment and prognosis of infants with retinoblastoma: a multicenter, 10-year retrospective analysis. BMC Pediatrics. 2023; 23: 229. https://doi.org/10.1186/s12887-023-03984-5.

[6] Ali MJ, Parsam VL, Honavar SG, Kannabiran C, Vemuganti GK, Reddy VAP. RB1 gene mutations in retinoblastoma and its clinical correlation. Saudi Journal of Ophthalmology: Official Journal of the Saudi Ophthalmological Society. 2010; 24: 119–123. https://doi.org/10.1016/j.sjopt.2010.05.003.

[7] Jin ZB, Xu J, Li B. Reflection on the origin and pathogenesis of retinoblastoma. [Zhonghua Yan Ke Za Zhi] Chinese Journal of Ophthalmology. 2024; 60: 883–886. https://doi.org/10.3760/cma.j.cn112142-20240724-00316. (In Chinese)

[8] Erdoğan ÖŞ, Ödemiş DA, Kayım ZY, Gürbüz O, Tunçer ŞB, Kılıç S, *et al*. Investigation of the methylation changes in the promoter region of RB1 gene in retinoblastoma: Unraveling the epigenetic puzzle in retinoblastoma. Pathology, Research and Practice. 2024; 253: 154939. https://doi.org/10.1016/j.prp.2023.154939.

[9] So JY, Pershing S, Pollom EL, Hiniker SM, Afshar AR. Disparities in United States Retinoblastoma Presentation, Management, and Local Recurrence in the National Cancer Database, 2004-2016. Ophthalmology. Retina. 2025; 9: 465–475. https://doi.org/10.1016/j.oret.2024.11.005.

[10] Huang X, Xia K, Wei Z, Liu W, Wei Z, Guo W. SLC38A5 suppresses ferroptosis through glutamine-mediated activation of the PI3K/AKT/mTOR signaling in osteosarcoma. Journal of Translational Medicine. 2024; 22: 1004. https://doi.org/10.1186/s12967-024-05803-6.

[11] Bhutia YD, Mathew M, Sivaprakasam S, Ramachandran S, Ganapathy V. Unconventional Functions of Amino Acid Transporters: Role in Macropinocytosis (SLC38A5/SLC38A3) and Diet-Induced Obesity/Metabolic Syndrome (SLC6A19/SLC6A14/SLC6A6). Biomolecules. 2022; 12: 235. https://doi.org/10.3390/biom12020235.

[12] Araya S, Kuster E, Gluch D, Mariotta L, Lutz C, Reding TV, *et al*. Exocrine pancreas glutamate secretion help to sustain enterocyte nutritional needs under protein restriction. American Journal of Physiology. Gastrointestinal and Liver Physiology. 2018; 314: G517–G536. https://doi.org/10.1152/ajpgi.00135.2017.

[13] Taurino G, Chiu M, Bianchi MG, Griffini E, Bussolati O. The *SLC38A5*/SNAT5 amino acid transporter: from pathophysiology to pro-cancer roles in the tumor microenvironment. American Journal of Physiology. Cell Physiology. 2023; 325: C550–C562. https://doi.org/10.1152/ajpcell.00169.2023.

[14] Kim MJ, Kim HS, Kang HW, Lee DE, Hong WC, Kim JH, *et al*. SLC38A5 Modulates Ferroptosis to Overcome Gemcitabine Resistance in Pancreatic Cancer. Cells. 2023; 12: 2509. https://doi.org/10.3390/cells12202509.

[15] Mathew M, Sivaprakasam S, Dharmalingam-Nandagopal G, Sennoune SR, Nguyen NT, Jaramillo-Martinez V, *et al*. Induction of Oxidative Stress and Ferroptosis in Triple-Negative Breast Cancer Cells by Niclosamide via Blockade of the Function and Expression of SLC38A5 and SLC7A11. Antioxidants (Basel, Switzerland). 2024; 13: 291. https://doi.org/10.3390/antiox13030291.

[16] Zhang X, Wang Q, Wang X, Chen X, Shao M, Zhang Q, *et al*. Tanshinone IIA protects against heart failure post-myocardial infarction via AMPKs/mTOR-dependent autophagy pathway. Biomedicine & Pharmacotherapy. 2019; 112: 108599. https://doi.org/10.1016/j.biopha.2019.108599.

[17] Oke I, Gonzalez E, Elze T, Miller JW, Lorch AC, Hunter DG, *et al*. The Association of Race, Ethnicity, and Insurance Status with the Visual Acuity of Retinoblastoma Survivors in the IRIS® Registry. Ophthalmic Epidemiology. 2025; 32: 18–24. https://doi.org/10.1080/09286586.2024.2315075.

[18] Cruz-Gálvez CC, Ordaz-Favila JC, Villar-Calvo VM, Cancino-Marentes ME, Bosch-Canto V. Retinoblastoma: Review and new insights. Frontiers in Oncology. 2022; 12: 963780. https://doi.org/10.3389/fonc.2022.963780.

[19] Ma X, Li X, Sun Q, Luan F, Feng J. Molecular Biological Research on the Pathogenic Mechanism of Retinoblastoma. Cur-

rent Issues in Molecular Biology. 2024; 46: 5307–5321. https://doi.org/10.3390/cimb46060317.

[20] Marković L, Bukovac A, Varošanec AM, Šlaus N, Pećina-Šlaus N. Genetics in ophthalmology: molecular blueprints of retinoblastoma. Human Genomics. 2023; 17: 82. https://doi.org/10.1186/s40246-023-00529-w.

[21] Rathore S, Verma A, Ratna R, Marwa N, Ghiya Y, Honavar SG, *et al*. Retinoblastoma: A review of the molecular basis of tumor development and its clinical correlation in shaping future targeted treatment strategies. Indian Journal of Ophthalmology. 2023; 71: 2662–2676. https://doi.org/10.4103/IJO.IJO_3172_22.

[22] Sniegowski T, Korac K, Bhutia YD, Ganapathy V. SLC6A14 and SLC38A5 Drive the Glutaminolysis and Serine-Glycine-One-Carbon Pathways in Cancer. Pharmaceuticals (Basel, Switzerland). 2021; 14: 216. https://doi.org/10.3390/ph14030216.

[23] Huang Y, He J, Chen N, Du X, Peng J. ETV4 promotes the growth, metastasis, glycolysis, and oxaliplatin resistance of colorectal cancer by transcription activation-mediated SLC38A5 upregulation. Pathology, Research and Practice. 2025; 271: 156033. https://doi.org/10.1016/j.prp.2025.156033.

[24] Wang S, Wu X, Bi W, Xu J, Hou L, Li G, *et al*. ROS-induced cytosolic release of mitochondrial PGAM5 promotes colorectal cancer progression by interacting with MST3. Nature Communications. 2025; 16: 1406. https://doi.org/10.1038/s41467-025-56444-2.

[25] He L, Cho S, Blenis J. mTORC1, the maestro of cell metabolism and growth. Genes & Development. 2025; 39: 109–131. https://doi.org/10.1101/gad.352084.124.

[26] Allegrini S, Camici M, Garcia-Gil M, Pesi R, Tozzi MG. Interplay between mTOR and Purine Metabolism Enzymes and Its Relevant Role in Cancer. International Journal of Molecular Sciences. 2024; 25: 6735. https://doi.org/10.3390/ijms25126735.

[27] Li J, Zhang D, Wang S, Yu P, Sun J, Zhang Y, *et al*. Baicalein induces apoptosis by inhibiting the glutamine-mTOR metabolic pathway in lung cancer. Journal of Advanced Research. 2025; 68: 341–357. https://doi.org/10.1016/j.jare.2024.02.023.

[28] Shen X, Wang G, He H, Shang P, Yan B, Wang X, *et al*. SLC38A5 promotes glutamine metabolism and inhibits cisplatin chemosensitivity in breast cancer. Breast Cancer (Tokyo, Japan). 2024; 31: 96–104. https://doi.org/10.1007/s12282-023-01516-8.

[29] Sun X, Wang B, Ding L, Wang Y, Xu M. Analysis of hsa_circ_0136256 as a biomarker for fibrosis in systemic sclerosis. BMC Biotechnology. 2024; 24: 91. https://doi.org/10.1186/s12896-024-00910-0.

[30] Sniegowski T, Rajasekaran D, Sennoune SR, Sunitha S, Chen F, Fokar M, *et al*. Amino acid transporter SLC38A5 is a tumor promoter and a novel therapeutic target for pancreatic cancer. Scientific Reports. 2023; 13: 16863. https://doi.org/10.1038/s41598-023-43983-1.

[31] Laplante M, Sabatini DM. mTOR signaling in growth control and disease. Cell. 2012; 149: 274–293. https://doi.org/10.1016/j.cell.2012.03.017.

[32] Wyant GA, Abu-Remaileh M, Wolfson RL, Chen WW, Freinkman E, Danai LV, *et al*. mTORC1 Activator SLC38A9 Is Required to Efflux Essential Amino Acids from Lysosomes and Use Protein as a Nutrient. Cell. 2017; 171: 642–654.e12. https://doi.org/10.1016/j.cell.2017.09.046.

[33] Rebsamen M, Pochini L, Stasyk T, de Araújo MEG, Galluccio M, Kandasamy RK, *et al*. SLC38A9 is a component of the lysosomal amino acid sensing machinery that controls mTORC1. Nature. 2015; 519: 477–481. https://doi.org/10.1038/nature14107.

[34] Choudhury M, Schaefbauer KJ, Kottom TJ, Yi ES, Tschumperlin DJ, Limper AH. Targeting Pulmonary Fibrosis by SLC1A5-Dependent Glutamine Transport Blockade. American Journal of Respiratory Cell and Molecular Biology. 2023; 69: 441–455. https://doi.org/10.1165/rcmb.2022-0339OC.

[35] Zhao X, Petrashen AP, Sanders JA, Peterson AL, Sedivy JM. SLC1A5 glutamine transporter is a target of MYC and mediates reduced mTORC1 signaling and increased fatty acid oxidation in long-lived Myc hypomorphic mice. Aging Cell. 2019; 18: e12947. https://doi.org/10.1111/acel.12947.

[36] Sokolov AM, Holmberg JC, Feliciano DM. The amino acid transporter Slc7a5 regulates the mTOR pathway and is required for granule cell development. Human Molecular Genetics. 2020; 29: 3003–3013. https://doi.org/10.1093/hmg/ddaa186.

[37] Sun Y, Wen J, Xu T, Meng L. Reduction of peritoneal cavity B1a cells in adult Slc7a5 knockdown mice via dysregulating the mTOR pathway. International Immunopharmacology. 2023; 117: 109939. https://doi.org/10.1016/j.intimp.2023.109939.

[38] Unek G, Ozmen A, Mendilcioglu I, Simsek M, Korgun ET. The expression of cell cycle related proteins PCNA, Ki67, p27 and p57 in normal and preeclamptic human placentas. Tissue & Cell. 2014; 46: 198–205. https://doi.org/10.1016/j.tice.2014.04.003.